Journal of Applied Polymer Science

Understanding the mechanical and interfacial properties of core–shell structured bamboo–plastic composites

Yu Xian,[1] Cuicui Wang,[2] Ge Wang,[1] Wenhan Ren,[1] Haitao Cheng[1]

[1]State Forestry Administration Key Laboratory of Bamboo and Rattan Science and Technology, International Centre for Bamboo and Rattan, Beijing 100102, People's Republic of China

[2]Ministry of Education Key Laboratory of Wooden Material Science and Application, Beijing Forestry University, Beijing 100083, People's Republic of China

Correspondence to: H. Cheng (E-mail: htcheng@icbr.ac.cn)

ABSTRACT: Core–shell structured bamboo–plastic composites (BPCs) were directly prepared with a single-screw/single-screw coextruder system. The effects of different shell layers, such as high-density polyethylene (HDPE), bamboo pulp fiber (BPF)/HDPE, and white mud (WM)/HDPE, were studied in the context of the mechanical properties and the characteristics of the interfacial transition zone (ITZ) of BPC. The mechanical properties of the core–shell structured BPC were characterized by flexure, short-beam shear, and impact tests. The surface morphologies of BPC were analyzed with field emission scanning electron microscopy. The ITZ properties were studied with dynamic mechanical analysis and nano-indentation testing. The results show that the flexural properties, short-beam strength, and impact strength decreased profoundly in the presence of BPF or WM. The dynamic mechanical analysis results suggest that the ITZ properties decreased, as indicated by the reductions in the storage modulus, loss modulus, and loss factor; the nano-indentation results show that on the addition of BPF or WM, a gradient in the hardness and modulus of elasticity appeared across ITZ. © 2015 Wiley Periodicals, Inc. J. Appl. Polym. Sci. **2016**, *133*, 43053.

KEYWORDS: composites; mechanical properties; properties and characterization

Received 17 June 2015; accepted 14 October 2015
DOI: 10.1002/app.43053

INTRODUCTION

Recently, wood–plastic composites (WPCs) have been widely used in buildings, furniture, packaging, transportation, and automobiles.[1] However, with the rapid development of the market and customer demands for better products and performances, traditional WPCs have failed to deliver on specific quality requirements, such as higher mechanical properties and lower water absorption. These problems can effectively be solved by means of coextrusion technology. Coextrusion is a process in which two or more polymer materials are extruded together to produce different multilayered structures (e.g., pipes, panels, core–shell profiles).[2–4] The final products have shown excellent properties for different types of materials used. For example, to produce optimum performance and structures, necessary steps, such as coloring, covering of UV, moisture barrier addition, and the mixing of additives, can be realized by the simple design addition of one or more layers. In addition, coextrusion is suitable for the use of certain waste materials and, thereby, significantly reduces production costs.[5–8]

Because of its advantages, coextrusion technology has been recognized for its potential applications in wood/bamboo–plastic composites (BPCs).[9] Work focusing on the application of coextrusion in BPCs is very limited. Stark and Matuana[10,11] were the first to report core–shell structured WPCs with coextrusion technology. In their study, core–shell structured WPCs were proven to have reduced moisture affinity in comparison to that in traditional WPCs, whereas the flexural properties remained almost identical to those in the traditional counterpart. They further investigated the effects of the shell layer, blended with additives such as a compatibilizer, photostabilizer, and nano-TiO_2, on the environmental stability of WPC. The results also show that the moisture resistance and color stability of the synthesized core–shell structured WPC were improved. Jin and Matuana[12] studied the flexural properties of core–shell structured WPCs through the addition of carbon nanotubes in a pure poly(vinyl chloride) shell layer. As compared to a pure poly(vinyl chloride) shell, the combination of carbon nanotubes increased both the overall flexural strength and the flexural modulus. Yao and Wu[13] discussed the mechanical and water absorption performances of core–shell structured WPCs with different core layer compositions, shell layer thicknesses, and shell wood loadings. The final results indicate that the optimum

composite properties were achieved by a combination of a weak core layer and a good shell layer. Kim *et al.*[9] further studied the effects of the shell layer blended with treated precipitated calcium carbonate and wood fiber on the properties of core–shell structured WPCs with weak and strong core systems. In their cases, as compared to the core-only composites, the flexural strength increased significantly for a reinforced shell in the weak core system, whereas the same decreased for the strong core system. At low filler contents in the shell, the impact strengths were significantly improved for both types of core systems.[9] Huang[14] studied the effects of the thickness of the shell layer and the type of fillers (talc and glass fiber) on the flexural properties and thermal performance of core–shell structured WPCs. In Huang's study, a finite-element based model was used to predict the coefficient of linear thermal expansion as a function of the shell thickness. Xiong *et al.*[15] investigated the elastic modulus (E), strength, and thermal expansion performance of core–shell structured WPCs; the results demonstrate the suitability of the composites for structural engineering applications via an optimized design.

However, the core–shell structured WPC–BPC was formed by a combination of wood fiber, bamboo fiber, or bamboo residue with various plastics through the coextrusion technology. The main problem here is the incompatibility between the hydrophilic fiber and hydrophobic plastic; this has led to their poor interfacial bonding quality and weak mechanical interaction.[1] Altun *et al.*[16] investigated the effect of pre-impregnation with a dilute polylactic acid (PLA) solution on the final properties of PLA-based composites. In their case, dynamic mechanical analysis revealed that the alkaline treatment and pre-impregnation reinforced the interface between the matrix polymer and filler. Son *et al.*[17] analyzed different additives for their effect on the dynamic mechanical properties of various WPCs and calculated the apparent activation energy of the same. The results indicate that for good dispersion or good adhesion at the interface, the development of the filler-reinforced polymer had a higher apparent activation energy.

Nano-indentation testing is a new approach for measuring the size and relative mechanical properties of the interphases. This technique has been applied to the interfacial properties of fiber-reinforced composite systems, such as glass- or carbon-fiber-reinforced thermally cured resins and thermoplastic matrix-based composite systems.[18–21] Very few studies have been performed in the direction of nano-indentation measurement at the interphase in natural-fiber-reinforced polymer composite systems. Lee *et al.*[22] investigated the mechanical properties of the interphase in cellulose-fiber-reinforced polypropylene (PP) composites with nano-indentation. On the basis of their results of nano-indentation, they concluded that the apparent width of the property transition zone might have been less than 1 μm. For the core–shell structured BPC, there also exited an identical interface between the core and shell layer. In this context, we defined the interface between the core and shell as the interfacial transition zone (ITZ). The ITZ is different for different shell materials, and the ITZ has a significant impact on the overall behavior and performance of the core–shell structured BPC.[14] So far, few works have been reported on the mechanical and interfacial properties of core–shell structured BPCs. In this study, we elucidated the effects of bamboo pulp fiber (BPF) and white mud (WM) filler shell layers on the mechanical and interfacial properties of core–shell structured BPCs.

EXPERIMENTAL

Materials and Preparation

Bamboo residue (BR), BPF, and WM were supplied by Guizhou Chitianhua Co., Ltd. (Chishui, China). The lubricant polyethylene (PE–wax) was obtained from Yi-Li Chemical Reagent Co. (Beijing, China); it was used to improve the processing of the BPC profile. Virgin high-density polyethylene (V-HDPE; DGDK-3364, density = 0.945 g/cm^3, melt flow index = 0.075 g/min at 190°C and 2.16 kg, a tensile strength = 22.1 MPa) was provided by Zhangmutou Plastic Co., Ltd. (Guangzhou, China). The compatibility of fiber–plastic blends were improved with the addition of maleic anhydride in the form of maleated polyethylene (MAPE; CMG9801), which was also acquired from Zhang Mu Tou Co., Ltd. (Guangzhou, China). BR and BPF were dried at 80°C for 24 h before blending with V-HDPE. WM was ground to 800-mesh before blending with other materials. Before the coextrusion process, the core and shell systems were pelletized with a twin-screw extruder at 150, 160, 165, 175, and 150°C die temperatures. V-HDPE and BR were used as core systems. The materials used for the shell were V-HDPE (CSHDPE), BPF/high-density polyethylene (HDPE) (CSBPF), and WM–HDPE (CSWM), with abbreviations of the corresponding core–shell structured BPC being CSHDPE, CSBPF, and CSWM, respectively.

Core–Shell Structured BPC Manufacturing

The composites were formulated with three shell types per core system. The core system was V-HDPE-BR-MAPE-PE–wax = 65:30:4:1 wt % PE–wax. The three shell types were V-HDPE–MAPE-PE–wax = 95:4:1 wt % PE–wax, V-HDPE–BPF–MAPE:PE–wax = 90:5:4:1 wt % PE–wax, and V-HDPE-WM-MAPE-PE–wax = 90:5:4:1 wt % PE–wax, respectively. The composites were manufactured with a coextrusion system. The system consists of a 30-mm single-screw extruder (Shanghai Sunlight Plastic Machinery Manufacturing Co., Ltd.) for the core and a 20-mm single-screw extruder (Shanghai Sunlight Plastic Machinery Manufacturing Co., Ltd.) for the shell. A specially designed die with a cross-sectional area of 4 × 30 mm^2 was used in combination with the core, and the shell thickness was controlled by the adjustment of the core–shell extruder rotational speed ratio to 1:2. The manufacturing temperatures at the die for the core systems were 160, 165, 170, 170, and 165°C; the same for the shell formulations were from 160 to 180°C. The coextruded BPCs were cooled with a 2-m water tank with a controlled water spray. The extrusion speed was maintained by a speed-controlled puller. The details can also be found in the literature.[2,4,8,15]

Characterization of the Core–Shell Structured BPC

Mechanical Properties. Three-point flexural testing was conducted with an Instron testing machine (model 5848) at a crosshead speed of 17 mm/min at ambient temperature according to ASTM D 790-10. The sample dimensions were 80 × 30 × 4 mm^3 (Length × Width × Thickness). Six samples were tested for each group. The short-beam shear strength of the

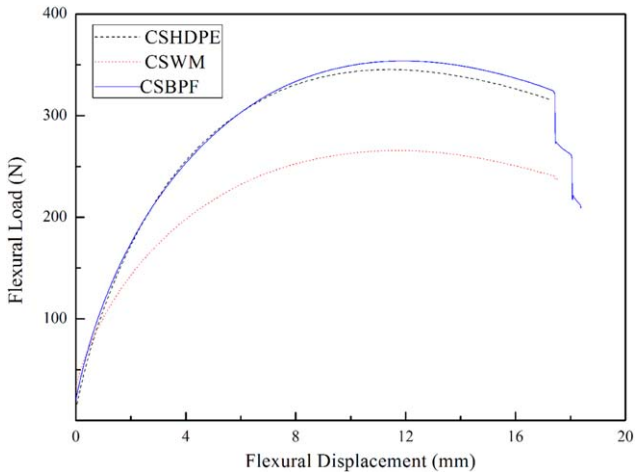

Figure 1. Effects of shell materials on the load–displacement curve of the core–shell structured BPC. [Color figure can be viewed in the online issue, which is available at wileyonlinelibrary.com.]

composites, as measured with the model 5848 Instron testing machine, was in accordance with JC/T773-2010/ISO14130:1997. The corresponding sample dimensions were 40 × 30 × 4 mm^3 (Length × Width × Thickness). The support span and testing speed were set at 20 mm and 5 mm/min, respectively; five samples per composition were tested. Charpy impact test were performed according to ASTM D 6110-10 with a pendulum hammer impact tester (Kecheng Testing Machine Co., Ltd. Chengde, China); five samples per composition were tested.

Morphological Studies. The surface of the core–shell structured BPCs was investigated with a field emission scanning electron microscope (JEOL-6310F) at an acceleration voltage of 7.0 kV. Before the examination, the surface was sputter-coated with a thin gold–palladium layer in a vacuum chamber to prevent charging.

Interfacial Properties of the Core–Shell Structured BPCs. ITZ was determined for rectangular specimens (60 × 14 × 4 mm^3; Length × Width × Thickness) with a dynamic mechanical analyzer (Q800, TA Instruments) in a dual-cantilever fixture (frequency = 1–10 Hz, strain amplitude = 30 μm).

Nano-Indentation Tests. Quasi-static indentation tests (MTS) were performed under ambient environmental conditions. In a force controlled mode, the indenter tip (Berkovich-type triangular pyramid) was loaded to a peak force of 250 μN at a loading rate of 50 μN/s, held at constant load for 6 s, and unloaded at a rate of 50 μN/s. The hardness (H) and E values were calculated from the load–displacement data.[22,23] As the indenter penetrated into the sample, both elastic and plastic deformation occurred, and only the elastic portion of the displacement was recovered during the unloading step. In nano-indentation, H is defined as follows:

$$H = \frac{P_{max}}{A} \quad (1)$$

where P_{max} is the peak load and A is the contact area.

The sample elastic modulus (E_s) could then be calculated as follows:

$$E_s = (1-\nu_s^2)\left(\frac{1}{E_r} - \frac{1-\nu_i^2}{E_i}\right)^{-1} \quad (2)$$

where ν_s is Poisson's ratio of the sample; E_i and ν_i are the values for the same indenter tip, and E_r is the reduced elastic modulus.

RESULTS AND DISCUSSION

Mechanical Properties

Figures 1 and 2 show the effects of the shell layers (BPF–HDPE and WM–HDPE) on the load–displacement curve, flexural modulus, and strength of the core–shell structured BPCs, respectively, as evaluated from the load–distance curves. As shown in Figure 1, that the deflection linearly increased with increasing load before the core–shell structured BPC yields. After this, the slope of the load-deflection curves decreased gradually. It was also clear that the three core–shell structured BPCs presented here showed profound failure modes: ductile failure and brittle failure. This showed that the mixing of BPF in the shell layer improved the ductility of the core–shell structured BPCs and reduced the brittle failure, mainly because of bending.

As shown in Figure 2, the flexural strength and modulus of the core–shell structured BPCs decreased with the addition of BPF or WM. The flexural strength and modulus of CSHDPE were higher than those of CSWM and CSBPF. The degradation in the flexural modulus and strength of the core–shell structured BPCs might have been critical to the poor interfacial adhesion in ITZ. This was due to the fact that the properties of the shell layer (V-HDPE) were similar to those of the core layer, and the interfacial compatibility between the core and shell was better. Compared with CSWM, the addition of MAPE effectively improved the compatibility of BPF and V-HDPE and, hence, MAPE showed good bonding with V-HDPE. The flexural modulus of the sample CSWM was lower than those of CSHDPE and CSBPF, the results agreed with Figure 1. The primary component of WM was calcium carbonate, and the associated particle size distribution had a wide range (700 nm to 50 μm) with a mean diameter of 12.125 μm. WM was hybridized with microparticles/nanoparticles.[24] The compatibility of the core and shell layer was affected by the poor dispersion of WM in

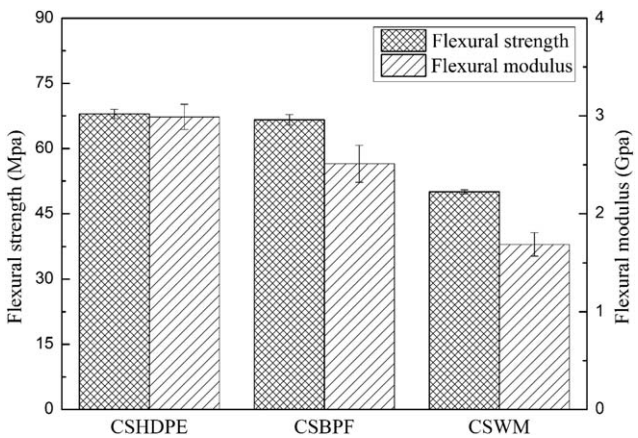

Figure 2. Effects of shell materials on the flexural modulus and strength of the core–shell structured BPC.

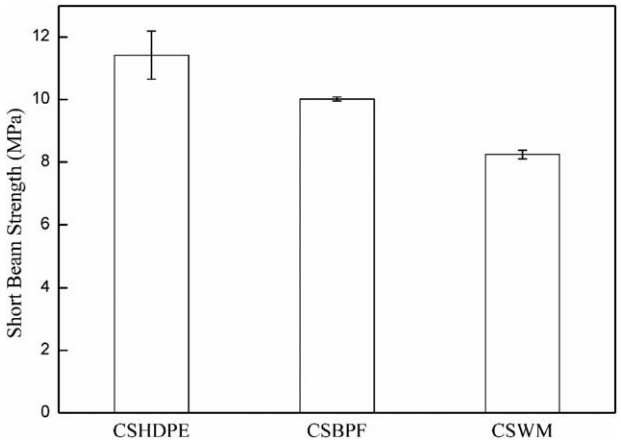

Figure 3. Effects of shell materials on the short-beam shear strength of the core–shell structured BPC.

V-HDPE. According to Mohd Zulfli *et al.*,[25] nanosized $CaCO_3$, because of its larger surface area, gives better reinforcing effects in comparison to the microsized $CaCO_3$. The studies from refs. 9 and 14 also proved that the shell material had an important effect on the mechanical properties of the core–shell structured BPCs. To explain the degradation phenomena of BPF and WM on the flexural properties, one should consider the poorly dispersed BPF and WM and that the interfacial interaction between the core and shell layer is weakened. The results show that mechanical characteristics of the interface had a significant effect on the composites and its flexural properties specifically.

The ITZ characteristics played an important role in the mechanical properties of the core–shell structured BPCs. To evaluate the interfacial adhesion strength between the core and shell layer, the short-beam shear strength of the composites was measured. The influence of WM and BPF is shown in Figure 3. CSHDPE presented a trend of increased strength in comparison to CSBPF and CSWM; this suggested better adhesion and, hence, a stronger core–shell interfaces in the same. This was correlated with the reduced flexural properties, as discussed in the previous section. Indeed, the shell with V-HDPE could be improved by increasing the strength of the core and shell; this benefitted, for instance, from a lower void content in the core–shell interface or within the resin itself. Voids in WPCs are very common and difficult to eliminate because most of them are caused by poor compatibility between the fibers or by the addition of fillers and polymer throughout the extrusion process. Thus, the short-beam shear strength of CSBPF and CSWM are generally lower than that of CSHDPE.[26] Compared with CSWM, the addition of MAPE increased the interfacial compatibility between HDPE and BPF. In addition, the morphological structure of BPF was slender and cylinder shaped, with an average length of 1146.61 μm (high aspect ratio).[27] BPF could thus easily form a network structure in the V-HDPE matrix. Consequently, the interfacial adhesion of CSBPF was better than that of CSWM.

Figure 4 shows the impact strength of the core–shell structured BPCs with different shell-layer materials. We observed that the impact strength of the composites with V-HDPE was relatively higher than those of the other composites. According to Huang *et al.*,[14] the decrease in the impact strength of the core–shell structured BPCs may have been due to the fact that there was a poor interfacial adhesion between the core and the shell layer; this increased the stress concentration. Therefore, this required less energy for fracture fiber pullout from the matrix.[25] In particular, BPF and WM were susceptible to these degradation phenomena, which significantly affected the final properties in terms of the poor dispersion of BPF and WM in the shell layers.

As observed in the cross section of the BPCs, the mechanical performance of the core–shell structured BPCs was dependent on the quality of the core–shell adhesion. Figure 5(A-a) shows that there were almost no gaps in the core and shell layers. This morphology suggested that a better surface contact area between the core and shell was realized. The cross sections of core–shell structured BPC with BPF–HDPE shell materials are shown in Figure 5(A-b). We observed that the section of the core–shell structured BPCs became rougher with the presence of BPF. In general, sections showing fibers that are surrounded by a large quantity of matrix material are commonly associated with good fiber–matrix interfacial adhesion.[25] However, Figure 5(A-b) shows that the exposed fibers were more frequent for this sample. This may have indicated that the fibers were unevenly dispersed in HDPE. Figure 5(A-c) shows the scanning electron microscopy micrographs taken from the section of the composites with the WM–HDPE shell layer. We concluded that there were noticeable gaps (insufficient contact) between the core and shell layers. Small gaps observed at the interface revealed weak interfacial bonding. In other words, the poor mechanical properties were due to a lack of good interfacial bonding between the core and shell layers. This was correlated with the degradation of flexural properties, as discussed in the previous section. The degradation of the flexural properties of the core–shell BPCs were caused by the weak interfacial adhesion in the presence of BPF or WM. In other words, the BPF and WM had negative effects on the interfacial properties of the ITZ.

Figure 5(B) shows the impact-fractured surfaces of the core–shell structured BPCs. The picture of Figure 5(B-a) showed that

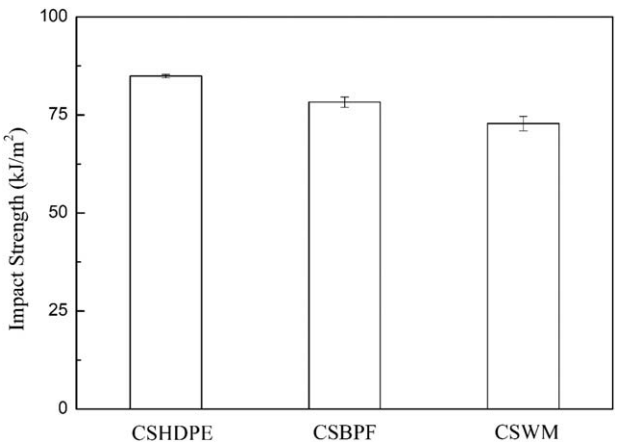

Figure 4. Effects of shell materials on the impact strength of the core–shell structured BPC.

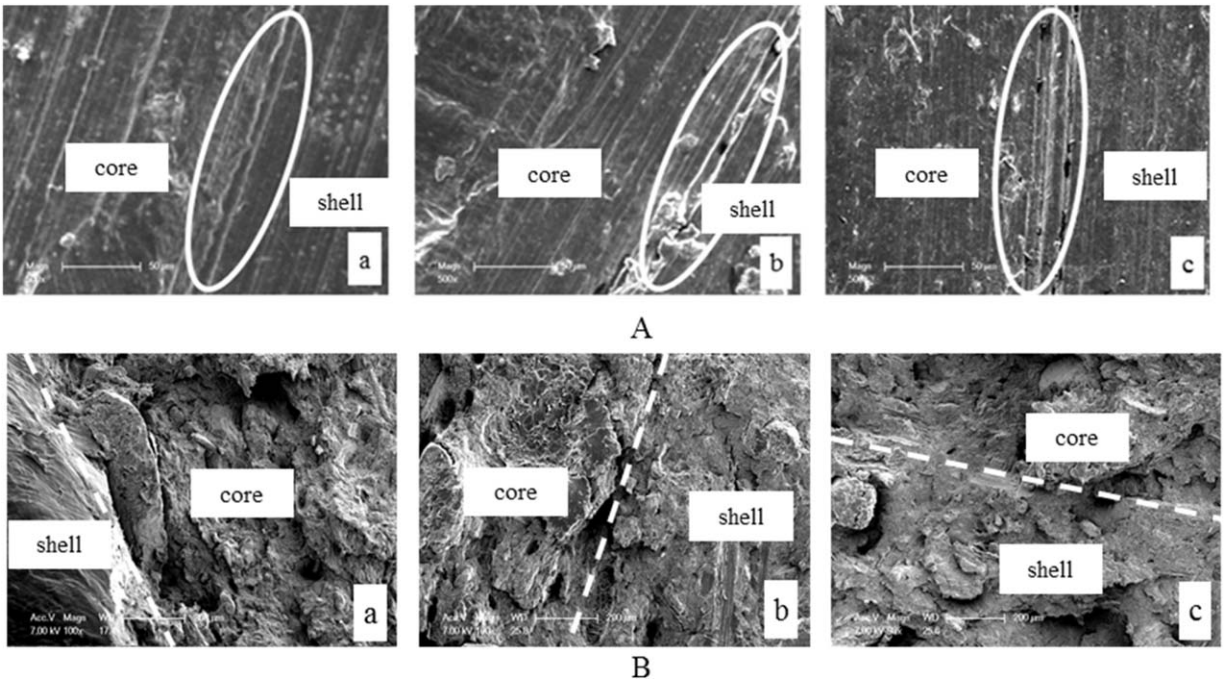

Figure 5. Scanning electron microscopy micrographs of the core–shell structured BPC: (A) cross section and (B) fractured surface of (a) CSHDPE, (b) CSBPF, and (c) CSWM.

the fractured section of V-HDPE was smooth. There were signs that, as shown in Figure 5(B-b), the BPF pulled out with the addition of BPF in the shell. As shown in Figure 5(B-c), when WM was loaded into the shell, the fractured section showed many defects, like holes. Even agglomerates began to appear; this was due to the fact that WM partly formed clusters or agglomerated structures in the HDPE matrix. The pullout and presence of voids in the fractured section were probably responsible for the poor mechanical and interfacial properties. These results were in agreement with reported in the literature.[24,28]

Interfacial Properties

Dynamic mechanical analysis was used to investigate the storage modulus (E'), E'', and mechanical loss factor (tan δ) of the composites under dynamic temperature or frequency conditions. The dynamic behavior of the polymer composites essentially reflected the structure of the composites, the relations between the molecular movement and performance, and the compatibility of each component in the composites. The total energy dissipation under cyclic load was divided into the core, shell layer, and interface between them. When the interfacial adhesion is poor, the continuous cyclic loading of composites resulted in a higher energy dissipation at the interface.[29]

Figure 6 shows the frequency dependence of E', E'', and tan δ for the core–shell structured BPCs. As shown, E' for the three composites increased with frequency, with the same being consistent at high frequency as compared to low frequency. In other words, the dynamic stiffness of the composites was higher than the static stiffness; this showed that the structure stability of the material was good under high frequency. This was due to the fact that under a constant force, the viscoelasticity of polymers was a function of the temperature, time, and frequency. As the external force was maintained at a constant value, the molecules of the composites decreased the effect of external stress through recombination. The molecule of the composites recombined quickly within a short period of time. So, the moduli of the composites at high-frequency loadings were higher than that for low-frequency loading.[30] Wang *et al.*[31] reported the thermodynamics of the mechanical properties of pultruded carbon fiber/vinyl ester resin composites, where we found that the improvement of interfacial properties caused E' and E'' to increase. The increase in E' of the core–shell structured BPC indicated that the composites exhibited better interactions between the core and the shell. This performance allowed the achievement of a higher modulus for CSHDPE. A similar observation was reported by Lin *et al.*[32] and Barick and Chang.[33] The highest value of the dynamic modulus was achieved for CSHDPE compared to those of CSBPF and CSWM. This tendency was statistically correlated to the bending test as well. In that way, there were imperfect interfaces between the core and shell layers in CSBPF and CSWM.

Figure 6(b) shows E'' values of the three composites, which decreased with increasing frequency. It is noteworthy that the E'' of the core–shell structured BPCs with a V-HDPE shell was higher than that of the other BPCs. The results indicate that the heat generated by molecular movement was lower; as a result, the energy loss in the composites was lower. A similar trend was observed in the tan δ of the composites, as shown in Figure 6(c). This was mainly related to the fact that the mechanical loss of the composites at high frequency was lower than that at low frequency. The tan δ of the composites decreased with increasing frequency. Generally, the energy dissipation of the core–shell structured BPCs involved the core, shell layer, and interfacial damping. Liu and Jiang[34] calculated the tan δ values

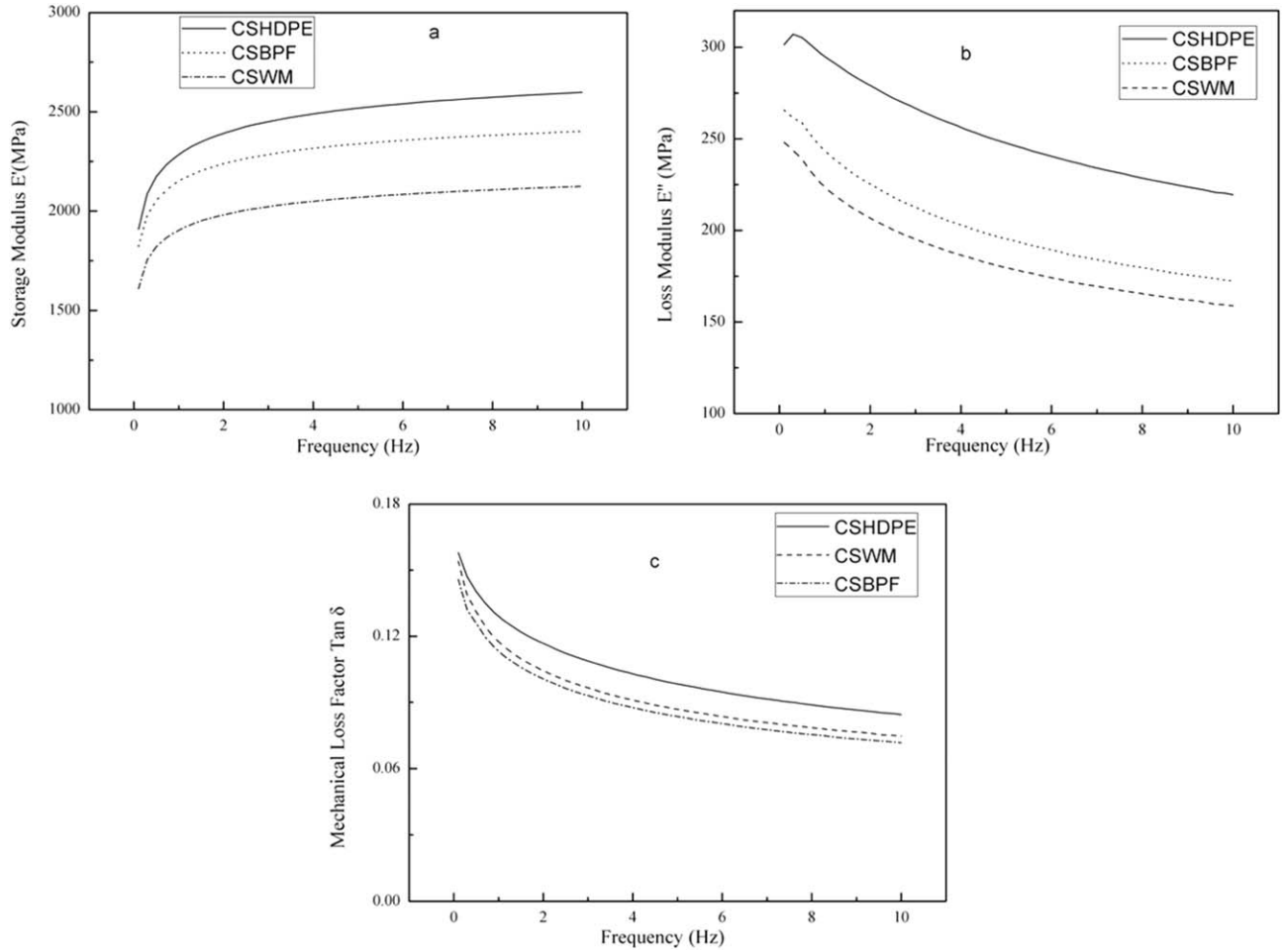

Figure 6. Effects of shell materials on (a) E', (b) E'', and (c) tan δ of the core–shell structured BPC.

of WPCs and evaluated the damping properties of the interface. The results show that the movement of the matrix chain segment was restricted because of the addition of bamboo powder; this made the damping performance degrade. At the same time, interfacial damping had significant effects on the damping properties of WPCs. The tan δ value of the CSHDPE composites was greater than those of CSBPR and CSWM at the same frequency. The influence of BPF and WM on the damping behavior of the core–shell structured BPCs was explained by two possible factors. One was the fact that the energy of the thermally activated molecular movement was different for the core–shell structured BPCs with different shell layers. The other factor might have been the fact that the incorporated BPF or WM restricted the mobility of the HDPE chains and had the tendency to render a higher elastic stiffness. The results were identical to those in the literature.[24]

A line of indents, spanning from the shell to the core layer, was made. The response nuances of nano-indentation were investigated in context of the ITZ properties variation. Seven test points were designed with 350 nm indentation depths. To prevent the overlapping of the impact zones of neighboring indents, the spacing of indentation was chosen to be a minimum of seven times the indentation depth.[35] The H and E values of the samples were obtained from the seven indentations at different locations, as shown in Figure 8. The figure also illustrates the profiles of E and H across the interphase regions; these were obtained after unloading at the final indentation. The mean E and H values of V-HDPE shell layer were 1.8–2.2 GPa and 0.12–0.14 GPa, respectively; the same values for the shell layer made with BPF–HDPE were 3.2–16 GPa and 0.18–0.8

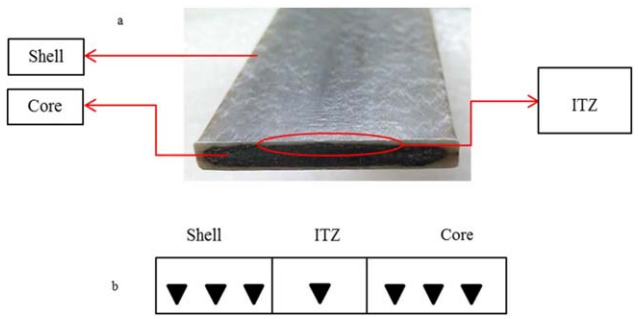

Figure 7. Relative position of ITZ: (a) diagram of ITZ and (b) position distribution of all depenetration in quasi-static nano-indentation. [Color figure can be viewed in the online issue, which is available at wileyonlinelibrary.com.]

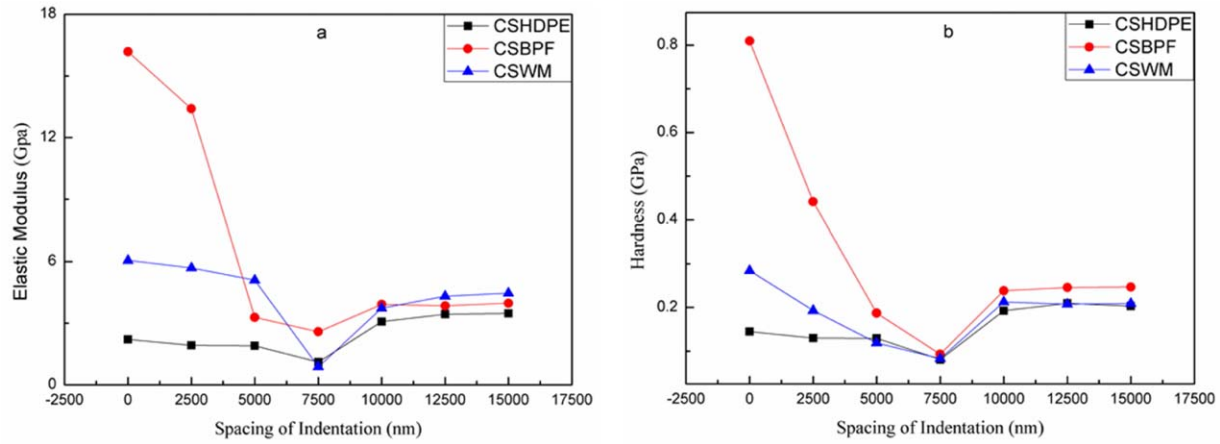

Figure 8. Effects of shell materials on *E* and *H* of the core–shell structured BPC: (a) *E* and (b) *H*. [Color figure can be viewed in the online issue, which is available at wileyonlinelibrary.com.]

GPa, respectively, whereas in the WM–HDPE shell system, they were 5–6 GPa and 0.11–0.28 GPa, respectively. The mean *H* and *E* values of the core layer were 0.19–0.25 GPa and 3–4.5 GPa, respectively. The values obtained in this study were similar to the reported values from Hodzic and coworkers.[22,36,37] One out of the seven indentations showed distinct *H* and *E* values in ITZ, with intermediate properties between those for the core and the shell (Figure 8). As evident, the corresponding values of *H* and *E* in ITZ were lower than the same values for the individual core and shell layer. This further illustrated that *E* and *H* of ITZ were different from those of the zones on either side. It was notable from the indentation made in ITZ that the properties of the indentation close to the core should have been affected less than those close to the shell. In other words, the results provided by these indents were more influenced by the different shell layer materials. The effect of the incorporation of BPF and WM on the ITZ properties of the core–shell structured BPCs could be partially explained as follows: when BPF and WM with high *E* values were well-dispersed through a low-*E* matrix, the modulus of the composites was obviously higher than that of the matrix. However, for the fillers in the shell to be really weak in nature, many other factors came into the picture, the most important being the force of adhesion of the core and shell layer, which played a crucial role. On the basis of these results, we concluded that the ITZ properties poorly contrasted with respect to the shell layer and the core.

CONCLUSIONS

On the basis of this study, which was devoted to the examination of influences of different shell materials on the interfacial and mechanical properties of core–shell structured BPCs, the following conclusions can be drawn.

The mechanical property tests revealed obvious differences between the different BPCs. The addition of WM or BPF showed significant effects on the flexural properties, short-beam shear strength, impact strength, and surface morphologies of the core–shell structured BPCs. The mechanical properties reached a maximum when the shell was HDPE in comparison to the addition of BPR or WM in the shell. A certain weakness of the interfacial bonds of ITZ was evidenced by scanning electron microscopy analysis of the cross section; this was not beneficial for the properties of the composites. In addition, the BPF pullout was always observed on the fracture surface, and impact fracture occurred at the sample sections where WM agglomeration was observed. At the same time, the ITZ properties of the core–shell structured BPCs were investigated by dynamic mechanical analysis and nano-indentation tests. The E', E'', and tan δ values of the core–shell structured BPCs showed a decrease in comparison to the HDPE-only shell. Nano-indentation was used to reveal the *H* and *E* values of the core and shell layers and ITZ in the composite materials. Compared with the core and shell layer, there was a significant difference among the *H* and *E* values in the ITZ; the mean values for *E* and *H* values for the BPF–HDPE shell were 2.58 and 0.09 GPa, respectively, whereas the values for the WM–HDPE shell were 0.88 and 0.08 GPa. These results demonstrate poor mechanical and interfacial properties for the core–shell structured BPCs prepared by the BPF–HDPE shell or WM–HDPE shell layer.

The mechanical and interfacial properties found in this study for the core–shell structured BPCs with BPF and WM in the shell layers were not significantly improved with respect to the HDPE ones currently used for shells. Thus, the final properties of the composites should be further improved by the optimization of the coextrusion process.

ACKNOWLEDGMENTS

The authors express sincere thanks to the State Forestry Administration Key Laboratory for Bamboo and Rattan Science and Technology and Tsinghua University. The authors also thank the pulp mills for providing the materials (Gui Zhou Chitianhua Group Co., Ltd.). This research was funded by the National Scientific and Technical Supporting 12th Five-Year Plan Project (grant 2012BAD23B0203) and the Fundamental Research Funds for the International Centre for Bamboo and Rattan (1632014002).

REFERENCES

1. Wang, Q. W.; Wang, W. H. Wood Plastic Composites and Products; Chemistry Industry: Beijing, **2006**; p 11.
2. Kirchmajer, D. M.; Gorkin, R.; Panhuis, M. *J. Mater. Chem. B* **2015**, *3*, 4105.
3. Negendank, M.; Mueller, S.; Reimers, W. *J. Mater. Process. Technol.* **2012**, *212*, 1954.
4. Koha, Y. H.; Kima, H. W.; Kima, H. E.; Hallorana, J. W. *J. Mater. Res.* **2003**, *18*, 2009.
5. Wang, L.; Shogren, R. L.; Carriere, C. *Polym. Eng. Sci.* **2000**, *40*, 499.
6. Mitsoulis, E. *J. Polym. Eng.* **2005**, *25*, 393.
7. Rowell, R. M. *J. Polym. Environ.* **2007**, *15*, 229.
8. Tzeng, G. C.; Chen, R. H. *Adv. Mater. Res.* **2014**, *939*, 381.
9. Kim, B. J.; Yao, F.; Han, G. P.; Wang, Q. W.; Wu, Q. L. *Compos. B* **2013**, *45*, 1040.
10. Stark, N. M.; Matuana, L. M. Proceedings of Coating Wood and Wood Composites: Journal of Architectural Coating: Washington, **2007**; p 23.
11. Stark, N. M.; Matuana, L. M. *Polym. Degrad. Stab.* **2004**, *86*, 1.
12. Jin, S.; Matuana, L. M. *Polym. Int.* **2010**, *59*, 648.
13. Yao, F.; Wu, Q. L. *J. Appl. Polym. Sci.* **2010**, *118*, 3594.
14. Huang, R. Z. Ph.D. Thesis, Nanjing Forest University, **2013**.
15. Xiong, W.; Wu, Q. L.; Cai, C. *S. Adv. Struct. Eng.* **2013**, *16*, 909.
16. Altun, Y.; Dogan, M.; Bayramlı, E. *J. Polym. Environ.* **2013**, *21*, 850.
17. Son, J.; Gardner, D. J.; O'Neill, S.; Metaxas, C. J. *Appl. Polym. Sci.* **2003**, *89*, 1638.
18. Gao, S. L.; Mader, E. *Compos. A* **2002**, *33*, 559.
19. Li, X.; Bhushan, B. *Mater. Char.* **2002**, *48*, 11.
20. Sridhar Babua, B.; Kumaraswamy, A.; Anjaneya Prasad, B. *Proc. Eng.* **2013**, *64*, 1048.
21. Tze, W. T. Y.; Wang, S.; Rials, T. G.; Pharr, G. *Compos. A* **2007**, *38*, 945.
22. Lee, S. H.; Wang, S. Q.; Pharr, G. M.; Xu, H. T. *Compos. A* **2007**, *38*, 1517.
23. Oliver, W. C.; Pharr, G. M. *J. Mater. Res.* **1992**, *7*, 1564.
24. Xian, Y.; Li, H. D.; Wang, C. C.; Wang, G.; Ren, W. H.; Cheng, H. T. *Bioresources* **2015**, *10*, 4263.
25. Mohd Zulfli, N. H.; Abu Bakar, A.; Chow, W. S. *High Perform. Polym.* **2014**, *26*, 223.
26. Ashori, A.; Shahrebabak, A. B.; Madhoushi, M. *J. Compos. Mater.* **2015**, *49*, 1107.
27. Ren, W. H.; Zhang, D.; Wang, G.; Cheng, H. T. *Bioresources* **2014**, *9*, 4117.
28. Colucci, G.; Ostrovskaya, O.; Frache, A.; Martorana, B.; Badini, C. *J. Appl. Polym. Sci.* **2015**, *132*, 42275.
29. Kennedy, J. M.; Edie, D. D.; Banerjee, A.; Cano, R. J. *J. Compos. Mater.* **1992**, *26*, 869.
30. Béhina, P.; Stocletb, G.; Rusec, N. D.; Sadound, M. *Dent. Mater.* **2014**, *30*, 728.
31. Wang, C. Z.; Yu, Y. H.; Yang, X. P.; Jin, R. G. *Acta Mater. Compos. Sin.* **2003**, *20*, 68.
32. Lin, L. Y.; Lee, J. H.; Hong, C. E.; Yoo, G. H.; Advani, S. G. *Compos. Sci. Technol.* **2006**, *66*, 2116.
33. Barick, A. K.; Chang, Y. W. *High. Perform. Polym.* **2014**, *26*, 609.
34. Liu, P. Y.; Jiang, Z. H. *Adv. Mater. Res.* **2013**, *815*, 639.
35. Guan, P. Q.; Li, Y. X.; Li, M.; Wang, J. *Fiber Reinforced Plastic/Composites* **2012**, *6*, 23.
36. Das, B.; Eswar, K.; Ramamurty, U.; Rao, C. N. R. *Nanotechnology* **2009**, *20*, 125705.
37. Hodzic, A.; Kim, J. K.; Stachurski, Z. H. *Polymer* **2000**, *41*, 6895.